– Report –

Refraction and reflection Seismic profilings to investigate Eocene arc - KY0715 cruise -

Narumi Takahashi[1]*, Tsutomu Takahashi[1], Shuichi Kodaira[1], Yoshiyuki Kaneda[1]

We carried out a deep wide-angle seismic experiment using a large airgun array and 110 ocean bottom seismographs (OBSs) along the Ogasawara Ridge from 26 November 2007 to December 25 (KY07-15 cruise) using R/V *Kaiyo* of the Japan Agency for Marine-Earth Science and Technology (JAMSTEC). The Ogasawara Ridge is an extinct arc that was produced in Eocene period. In addition, this arc collided with the Ogasawara Plateau and this event is expected to have severely deformed the crust. The objectives of this cruise are to understand the typical characteristics of the Eocene arc and the crustal deformation by collision with the Ogasawara Plateau. An airgun-OBS seismic line with a length of approximately 594 km was set along the Ogasawara Ridge through the gentle southern root near the collision point by the Ogasawara Plateau. We shot a large airgun array with a total volume of 12,000 cu. in. and recorded the seismic signals on OBSs with four components and a 12-channel hydrophone streamer. Moreover, we investigated the northern elongation of the Eocene arc by reflection survey using a G-gun array with a total capacity of 600 cu. in. and a 16-channel hydrophone streamer. In this paper, we summarize the seismic experiments and introduce the OBS data and reflection data.

Keywords : Crustal structure, seismic, wide-angle data, OBS, Izu-Ogasawara

---

Received 22 July 2008 ; accepted 2 October 2008

1 Japan Agency for Earth-Marine Science and Technology

Corresponding author:
Narumi Takahashi
Japan Agency for Earth-Marine Science and Technology (JAMSTEC)
3173-25, Showa-machi, Kanazawa-ku, Yokohama, 236-0001, Japan
+81-45-778-5372
narumi@jamstec.go.jp

Copyright by Japan Agency for Marine-Earth Science and Technology

1. Introduction

The Ogasawara Ridge crust is famous since it is an Eocene arc composed of boninitic materials (e.g., Ishizuka et al., 2006). The Eocene initial arc is located along the forearc region of the Izu-Ogasawara-Mariana arc, according to tectonic history (e.g., Karig and Moore, 1975; Hall et al., 1995; Macpherson and Hall, 2001; Honza and Fujioka, 2004). The frontal arc in the Mariana region, including Saipan and Guam, has been produced since the Eocene period; however, it is composed of not only an Eocene arc but also a Miocene one (Crawford et al., 1981). The Ogasawara Ridge is a purely Eocene arc and it is not contaminated by Miocene and current volcanisms (e.g., Honza and Fujioka, 2004). The ridge is therefore the best target that can be used to characterize the Eocene arc crust.

Determining the crustal structure of the Ogasawara Ridge is also important in understanding the crustal growth of the Izu-Ogasawara arc. The Izu-Ogasawara arc, which is a typical oceanic island arc with an andesitic middle crust with a P-wave velocity of 6 km/s, has been produced since the Eocene period. Two scenarios for the crustal growth in this region are proposed: one is that the current arc growth originated from basaltic primary magmas and the other is that an old initial arc in the Eocene period originated from the andesitic magmas. It is suggested that the crustal production rate in the Eocene period is several times that of the current arc volcanism (Stern and Bloomer, 1992); therefore, crustal growth in this region cannot be discussed without reference to Eocene volcanism.

The Eocene arc crust is composed of three layers, an upper crust with a velocity of 5.9–6.2 km/s, a middle crust with a higher velocity of 6.4–6.6 km/s and a lower crust with a velocity of 6.8–7.4 km/s (Takahashi et al., submitted). These velocities of the crustal layers are greater than those of the layer beneath the current volcanic front. This suggests that these crustal layers of the Eocene arc contain materials denser and more mafic materials than those beneath the volcanic front and that the Eocene arc includes considerably undifferentiated materials. Kodaira et al. (2007) indicated that the current volcanic arc exhibits remarkable along-arc velocity variations, suggesting that it differs in its stage of crustal growth between the northern and southern Izu-Ogasawara arcs. However, the structural characteristics of the whole Eocene arc crust, including the velocity variations along the arc, remain still not understood yet due to the small number of seismic experiments conducted in the region.

The Ogasawara Ridge abruptly reduces in altitude at 26°, and this could be due to deformation by collision with the Ogasawara Plateau. An alternative explanation for this reduction is that the Ogasawara Plateau might have subducted beneath the Ogasawara Ridge, resulting in the erosion of the base of the Ogasawara Ridge crust. The relationship between the Ogasawara Ridge and the plateau remains unknown.

The southern elongation of the Ogasawara Ridge also remains unknown. Fujioka et al. (2005) proposed that the Hahajima Seamount on the trench slope break of the Izu-Ogasawara Trench is a tectonic block and that it originated through the movement of the crustal block to the trench side due to the Parece Vela Basin opening. Based on this scenario, the southern elongation might have a crust similar to that of the oceanic crust, and it might exhibit drastic changes in crustal characteristics with respect to those for the Ogasawara Ridge.

The northern elongation of the Ogasawara Ridge has also remained an issue to be resolved. The Eocene arc developed with a large crustal production rate within about 10 Ma (Stern and Bloomer, 1992; Ishizuka et al., 2006), and the development is indispensable to subduction of the relatively warmer crust (e.g. Tatsumi, 2000). Therefore, the distribution of the northern end of the Eocene arc might lead to an understanding of the geologic environment of the subduction. Beneath the forearc region of the northern Izu arc, a middle crust with higher velocity of 6.0–6.5 km/s than that beneath the volcanic front was detected using a wide-angle seismic study (Takahashi et al., 1998), however, continuity of the crust with a high–velocity middle crust beneath the Izu forearc region north of the Ogasawara Ridge has remained ambiguous.

Here, we identify three scientific objectives to be resolved considering the abovementioned issues:

(1) crustal characterization and structural variation along the Eocene arc,

(2) detection of the drastic change or crustal deformation at the southern elongation of the Eocene arc crust, and

(3) the northern elongation of the Eocene arc.

To achieve these objectives, we carried out deep seismic profiling with 110 OBSs, a large airgun array, and a 12-channel streamer along a line on the Ogasawara Ridge rending N-S. In addition, other seismic reflection surveys using a 16-channel hydrophone streamer were conducted at the elongation of the Ogasawara Ridge.

2. Experiment

We performed a wide-angle seismic profiling along the Ogasawara Ridge using 110 ocean bottom seismographs (OBSs), a large airgun array with a capacity of 12,000 cu. in., and a 12-channel analogue streamer (Figure 1). The period of this cruise using the R/V *Kaiyo* of Japan Agency for Marine-Earth Science and Technology (JAMSTEC) was from 25 November 2007, to 25 December (Figure 2). A main seismic line runs along the eastern side of the Ogasawara islands, the Chichijima and the Hahajima Islands. The R/V *Kaiyo* departed from JAMSTEC on 26 November and we deployed 110 OBSs, shot the airgun, recovered all OBS, and conducted a multichannel seismic (MCS) survey using a G-gun array and a 16-channel streamer, as summarized in Table 1 and Figure 2. Finally, we arrived at JAMSTEC on 25 December.

2.1 Wide-angle refraction survey

We deployed 110 OBSs on the seismic line OGr1_obs with an interval of 5 km. To obtain good records using OBSs, we conducted airgun shooting with an interval of 200 m back and forth (lines OGr1_obs and OGr1_obsR). We then collected shot gather with an interval of 100 m. The airgun array with a total capacity of 12,000 cu. in. consisted of eight airguns (BOLT Technology Corporation, PAR Air Gun Model 1500LL) with a capacity of 1,500 cu. in. each. These guns were shot with the same timing within 1 ms. The gun depth was 10 m. We measured the shot times with an accuracy of 1 ns using a TrueTime system (TrueTime GPS time and frequency receiver, MODEL XL-AK). The air pressure imparted to the chamber was 2,000 psi. The geometry of the seismic experiment shown in Figure 4 is almost the same as that used in previous studies (e.g., Takahashi et al., 2003; Kaiho et al., 2005).

We retrieved 109 OBSs and lost one OBS (Figure 1, Table 3) due to an acoustic accident in the transponder system. All OBSs were equipped with three-component geophones with a natural frequency of 4.5 Hz (one vertical and two horizontal components perpendicular to each other) using gimbal-leveling mechanisms and a hydrophone sensor. The airgun signals through the crust and the mantle were digitized with intervals of 10 ms using a 16-bit A/D converter and they were continuously stored in their original format on a hard disk (Shinohara et al., 1993). Because these OBSs were deployed by free fall from the sea surface (Kanazawa and Shiobara, 1994), we measured their locations at the sea bottom using an acoustic receiver array with 16 components in total. The unevenness of the measured locations was a maximum 80 m. After recovering the OBSs, we edited the continuous OBS data with a length of 80 s and applied a correction for clock drift during deployment.

During the wide-angle refraction survey, we towed a 12-channel hydrophone streamer (Teledyne Mini-Streamer) to obtain the shallow sedimentary images. The group interval is 25 m and 16 sensors (Teledyne T2 Hydrophone) with sensitivity of 200 μV/μbar (pre-amplified 20 dB) are installed in one group. These analog signals recorded by 16 sensors are stacked, then digitized with a sampling of 4 ms. The depth of the streamer is 15 m and had been kept within ±2 m using three cable levelers (Digicourse, Digi Bird Model 5000). The recording system is the same as in previous studies (Takahashi et al., 2003). Digitized data is stored on DLT tape with a length of 13.5 s.

We used two differential global positioning systems (DGPSs): a Starfire system with a sampling interval of 1 s and a Skyfix system with a sampling interval of 4 s. The former was adopted as the main navigation system to control the gun shooting and the start of recording. During gun shooting, the variation was less than 10 cm and the position dilution of precision (PDOP) value was less than five. The number of GPS satellites was more than four, although satellites with an elevation of less than 10° were not used. The latter system, which was adopted as the vessel navigation system, was used as a secondary backup navigation system for the seismic experiment. The base station of the Skyfix was Okinawa, Japan.

2.2 Multichannel reflection survey

We also conducted an MCS survey using a G-gun array with a total capacity of 600 cu. in. in the forearc region of the northern Izu arc to achieve the following two major objectives (Figure 3). One was to understand the large–scale structure around the forearc region; the other was to determine the structure of sediments and the basement.

The large–scale structure around the forearc region, determined as the first objective, has remained an issue to be resolved. The forearc region includes many types of crustal structures. In addition, the elongation of the Eocene arc (the Ogasawara Ridge) and the extinct old rift (the Ogasawara Trough) and the detection of the old oceanic crust before the construction of the Eocene arc can be listed as unknown issues. Because we carried out seismic experiments in the forearc region along lines striking N-S (lines KT04 and KT04_s_0 on the KY0705 cruise), we set an MCS line (line KT04_s_1) connecting these lines with a strike of N-S.

In addition, we were yet to determine the fine structure of the sediments and the basement. JAMSTEC repeatedly recorded MCS data for the forearc region. However, the airgun array used as the source had a total capacity of 12,000 cu. in. and it was tuned for relatively deep structures. Although we planned another seismic experiment to obtain high resolution images and set eight seismic lines with a length of 100 km and an interval of 3 km, the seismic lines we finally considered were IBM2_ew5, IBM2_ew8, and IBM2_ew9.

We adopted the G-gun array (Sercel Inc., G. GUN 150) as the source to detect the structural changes between the Eocene arc and/or the oceanic crust. The G-gun array is composed of two linear clusters with two G-guns each (Figure 4b). Each G-gun has a chamber with a capacity of 150 cubic in. Because the spacing of

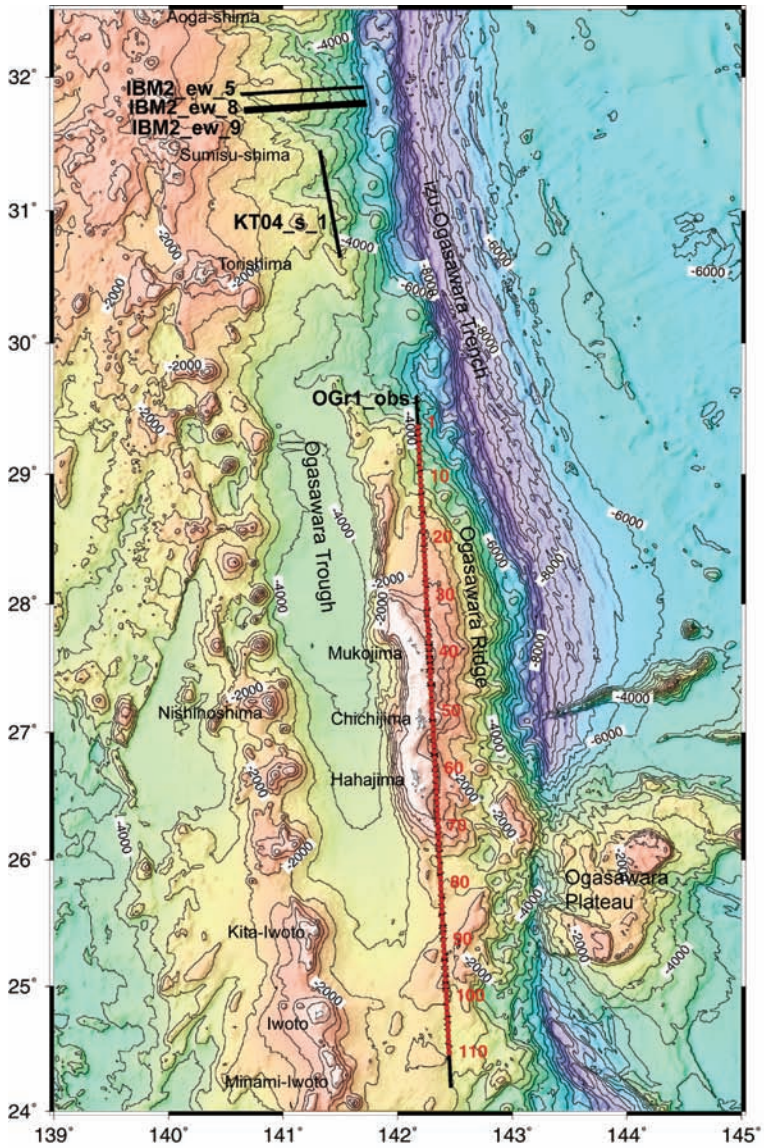

Figure 1. Topographic map of the experimental area. Red solid circles and black lines indicate OBSs and seismic lines, respectively. We shot an airgun array on line OGr1_obs and a G-gun array on lines KT04_s_1, IBM2_ew_5, IBM2_ew_8, and IBM2_ew_9. The interval of the contour line is 500 m.

each linear cluster is 3.5 m, the shot timing of these G-guns should be zero according to the G-gun shooting test. The shot timing using the G-guns was limited to less than 1 ms. The gun depth was 5 m. The shot time was measured using a TrueTime system. The air pressure of the chamber was 2,000 psi. The shot interval was 25 m and the shot timing was always controlled by the Starfire navigation system, similar to the case in the wide-angle survey.

The specifications of the hydrophone streamer are similar to those described in section 2.1. We selected a 16-channel stremaer to improve the resolution of the velocity analysis and set the depth of the streamer during shooting to 5 m so as to fit the properties of the source waveform for high–resolution imaging. The streamer depth was controlled within ±2 m by four cable levelers. The record length was 10 s and the sampling interval was 1 ms.

3. Data

In this chapter, we introduce some examples of the seismic data obtained by OBSs and MCS. The vertical components of Site5 at the northern Ogasawara Ridge, Site31 in the central part of the Ogasawara

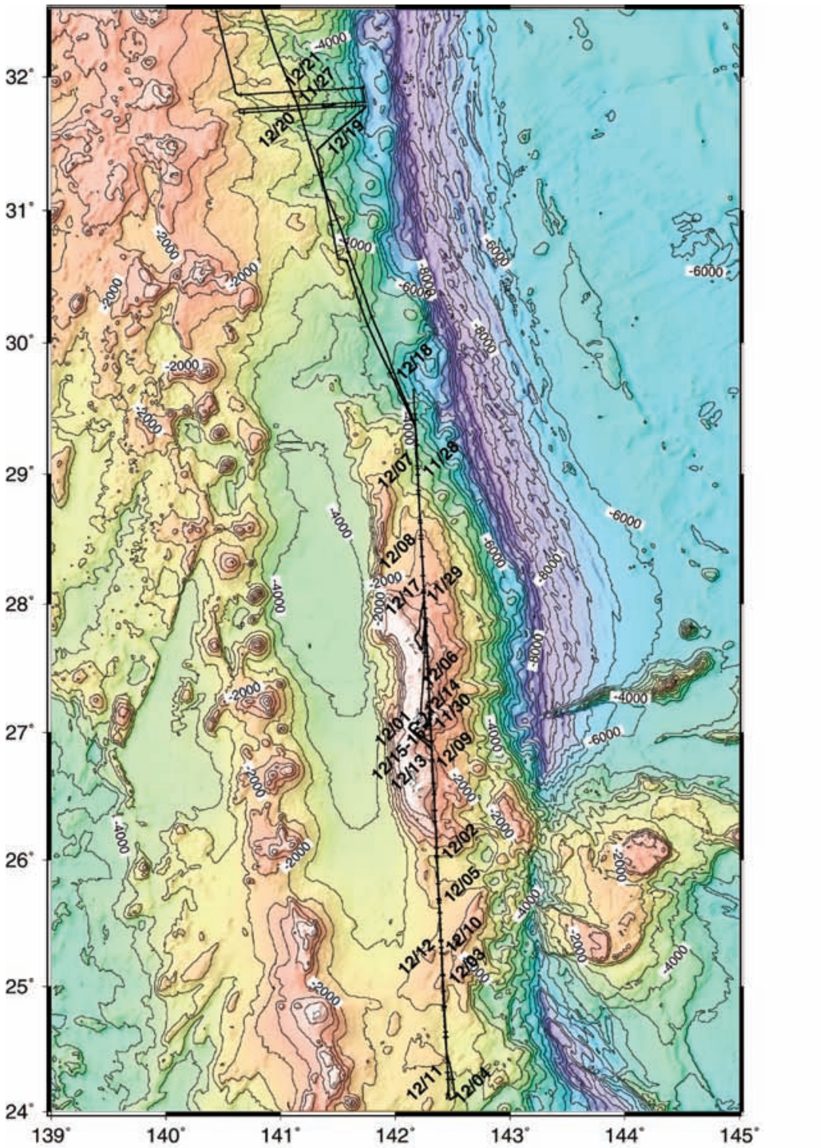

Figure 2. Ship's track line. Cross marks indicate ship position every 6 h. Numerals shown in the figure indicate the locations of the vessel at midnight each day (UTC). The interval of the contour line is 500 m.

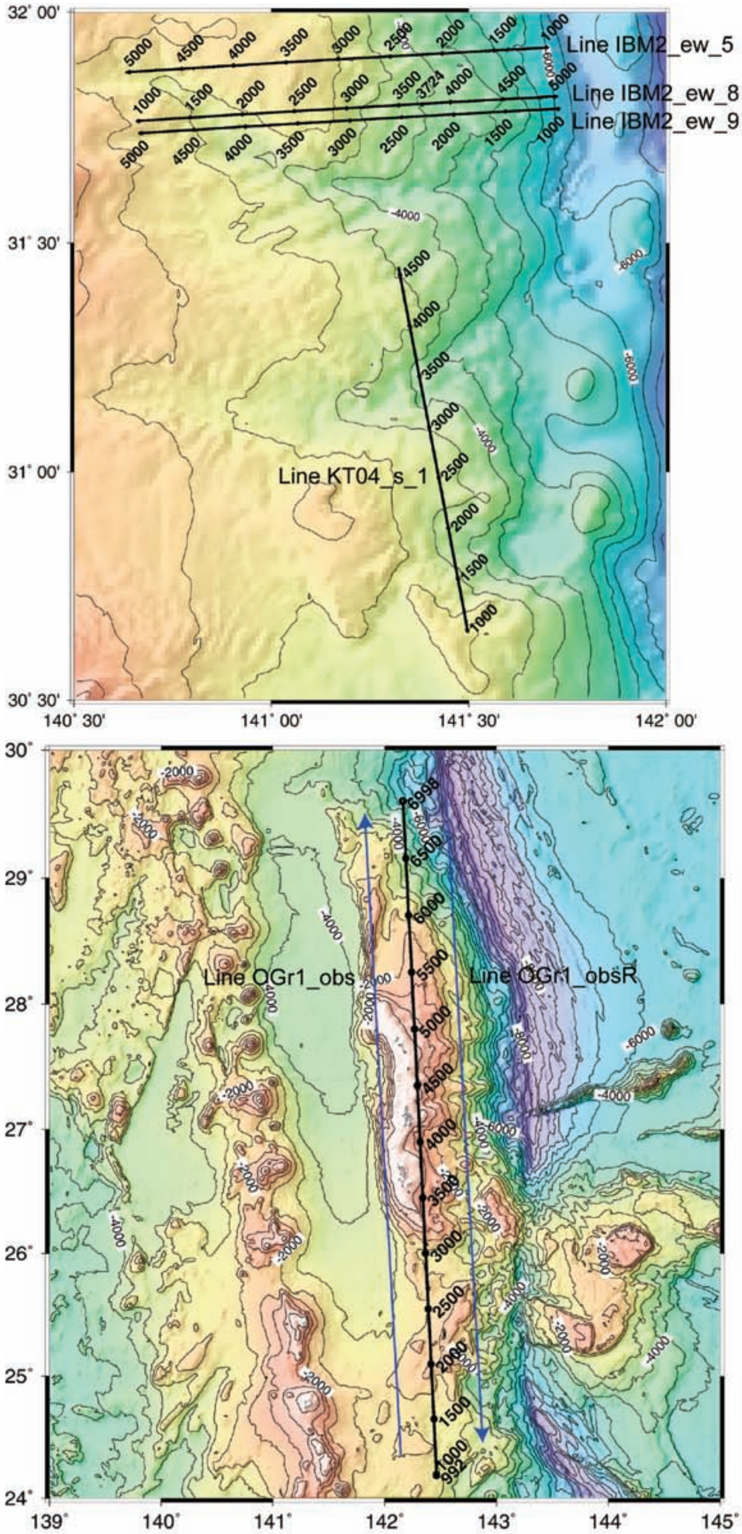

Figure 3. Map of airgun shooting in the forearc region of the northern Izu arc (up) and the Ogasawara Ridge (down). Blue arrows along line OGr1_obs show direction of shooting. Airgun shooting along line OGr1_obs was carried out twice (lines OGr1_obs and OGr1_obsR) to gather shots at an interval of 100 m. The interval of the contour line is 500 m.

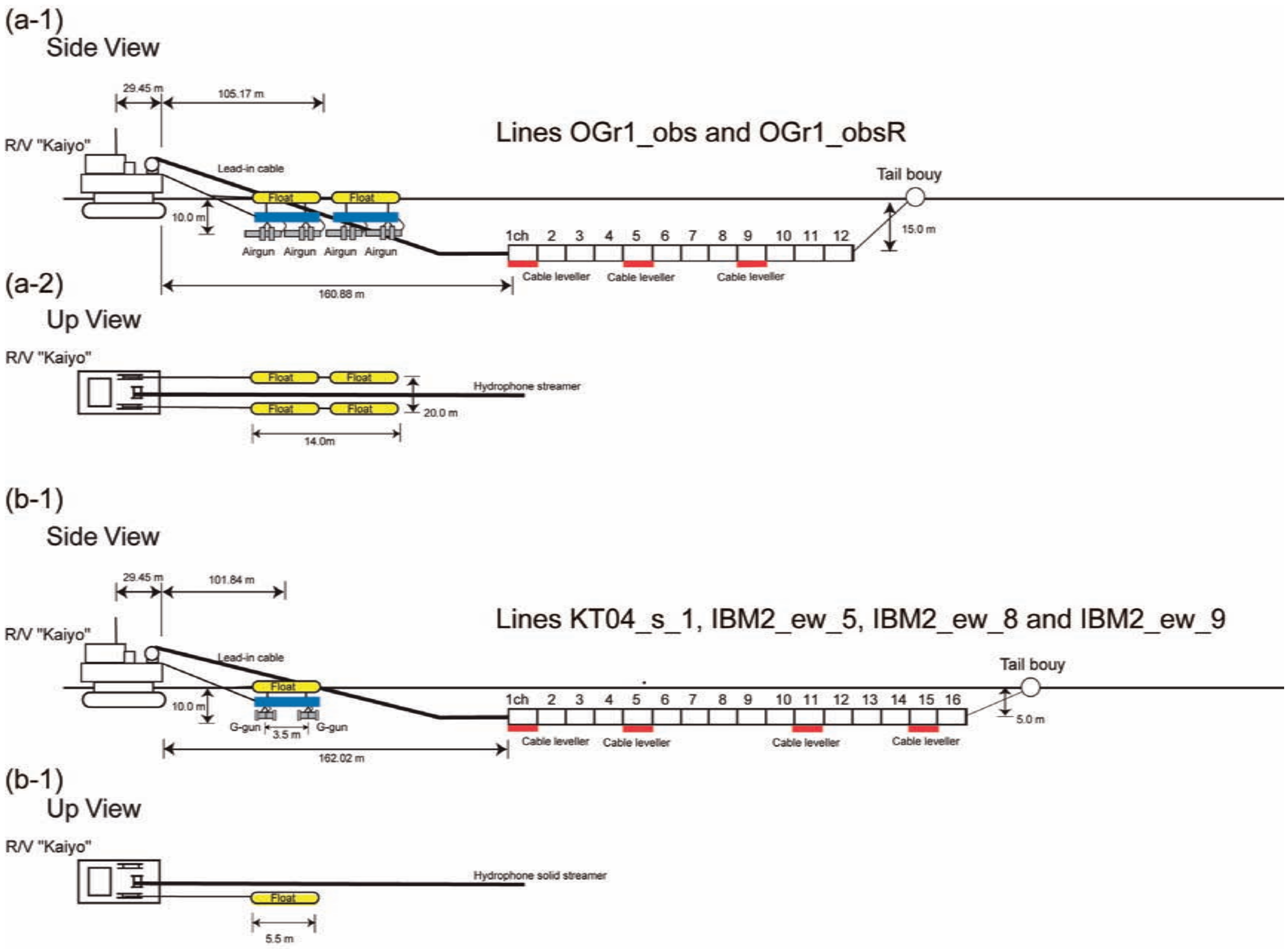

Figure 4. Side and top views for geometry of airgun system and the hydrophone streamer. (a-1) Side view of the geometry during gun shooting along lines OGr1_obs and OGr1_obsR. We towed a 12-channel streamer and an airgun array along these lines. (a-2) Top view of the geometry during gun shooting along the above–mentioned lines. (b-1) Side view of the geometry during gun shooting along lines KT04_s_1, IBM2_ew_5, IBM2_ew_8, and IBM2_ew_9. We towed a 16-channel streamer and a G-gun array along these lines. (b-2) Top view of the geometry during gun shooting along the above–mentioned lines.

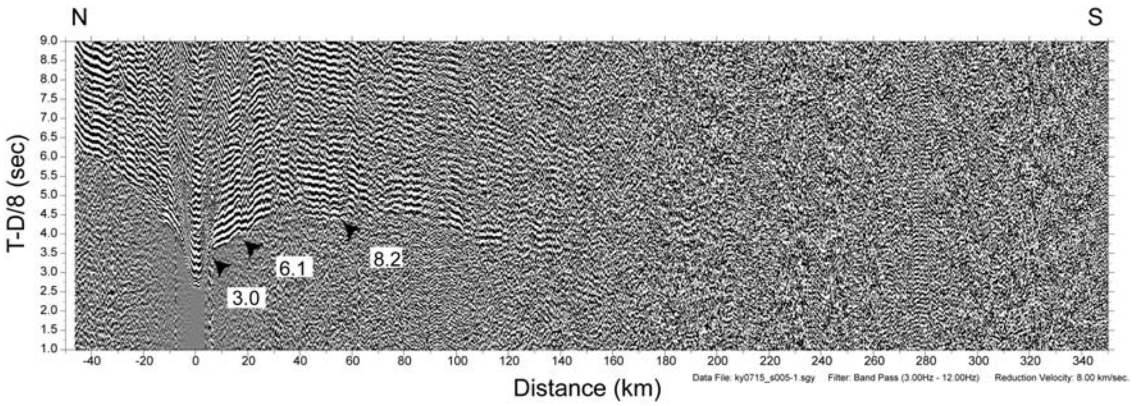

Figure 5. Vertical record section recorded by Site5. All traces are applied by a bandpass filter at 3-12 Hz. Vertical and horizontal axes are offsets (km) from OBS and travel times (s) reduced by 8 km/s. Numerals indicate apparent velocity (km/s).

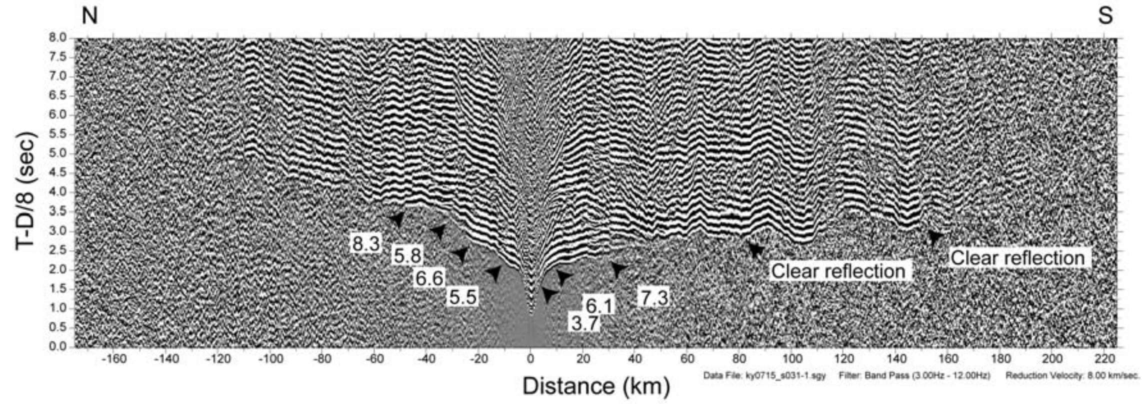

Figure 6. Vertical record section recorded by Site31. Details are the same as those for Figure 5.

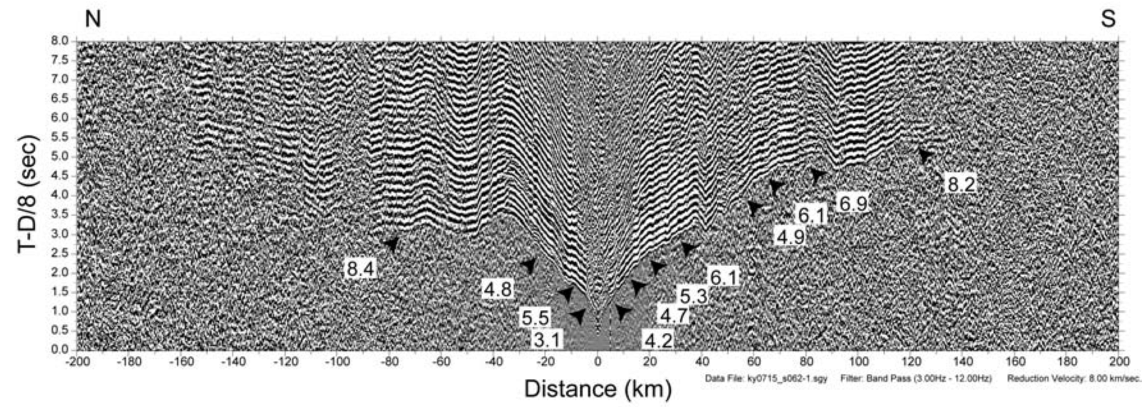

Figure 7. Vertical record section recorded by Site62. Details are the same as those for Figure 5.

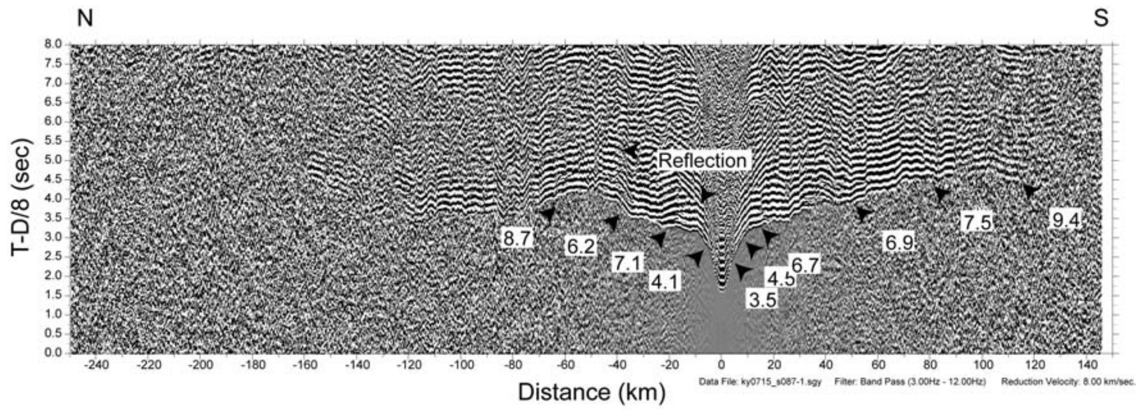

Figure 8. Vertical record section recorded by Site87. Details are the same as those for Figure 5.

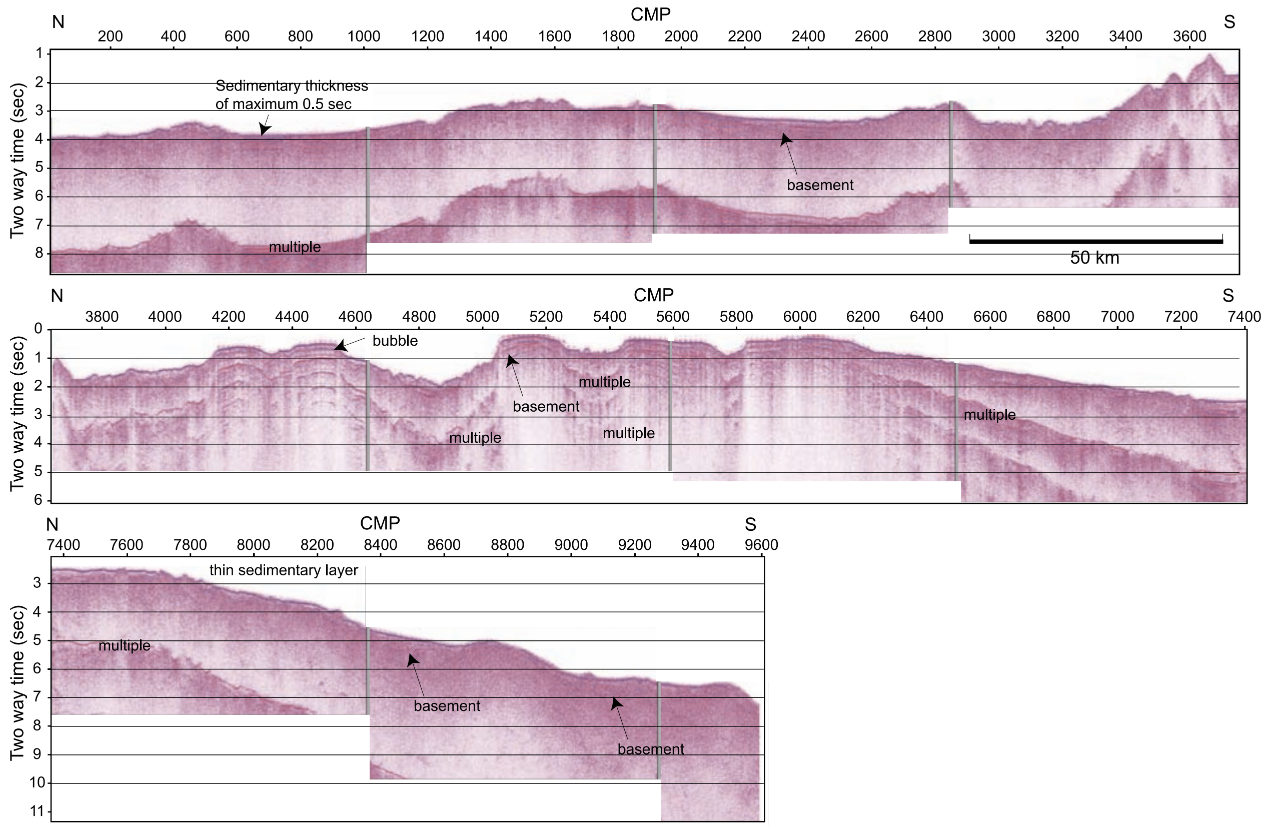

Figure 9. Time migrated section along line OGr1_obs. Horizontal and vertical axes are common mid point (CMP) and two–way travel time (s). Events indicated by “multiple” are multiple noises running between the sea bottom and the sea surface.

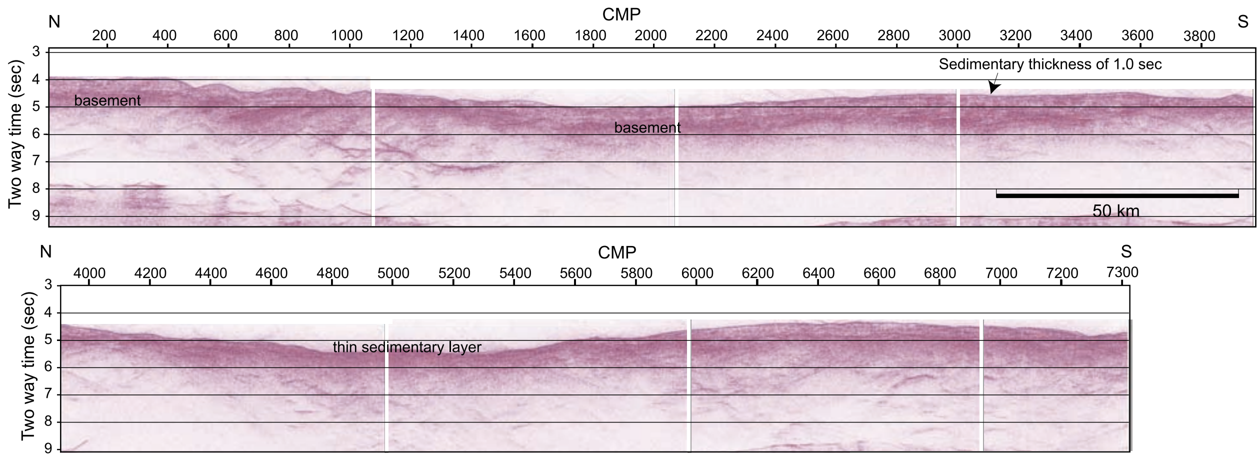

Figure 10. Time migrated section along line KT04_s_1. Details are the same as those for Figure 9.

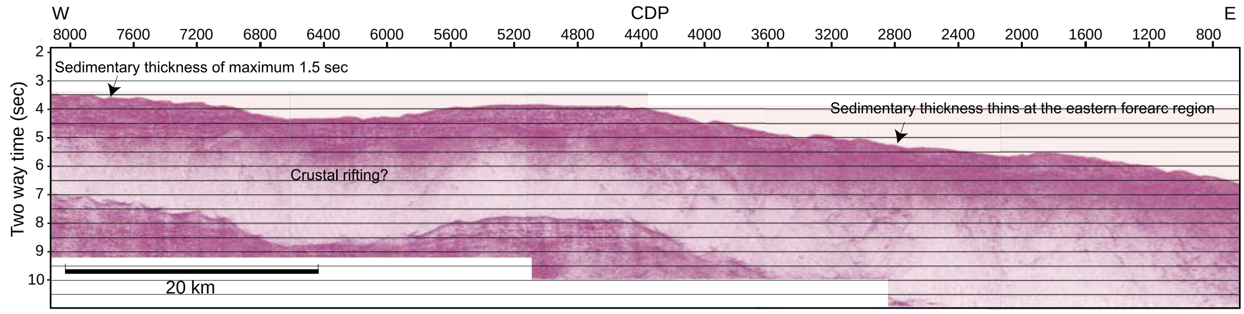

Figure 11. Time migrated section along line IBM2_ew_9. Details are the same as those for Figure 9.

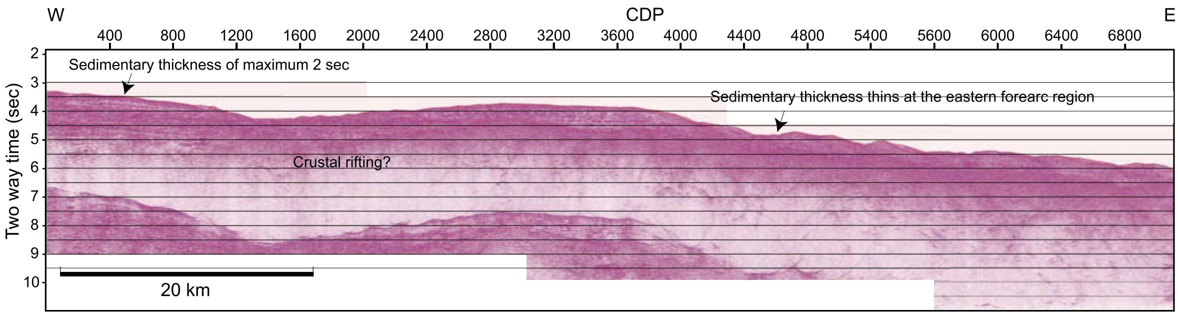

Figure 12. Time migrated section along line IBM2_ew_8. Details are the same as those for Figure 9.

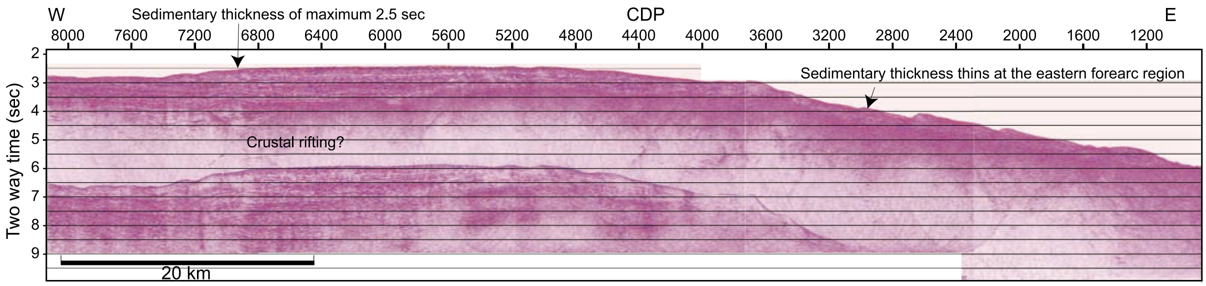

Figure 13. Time migrated section along line IBM2_ew_5. Details are the same as those for Figure 9.

Table 1. Activity log during the KY0511 cruise.

Date (UTC)	Remarks
November 26	Departure from JAMSTEC
November 27	Transit and OBS deployment (Site#1-Site#5)
November 28	OBS deployment (Site#6-Site#25)
November 29	OBS deployment (Site#26-Site#45), temporary wating due to bad sea status
November 30	OBS deployment (Site#46-Site#55) and evacuation due to bad sea status
December 01	Evacuation due to bad sea status and OBS deployment (Site#56-Site#72)
December 02	OBS deployment (Site#73-Site#92)
December 03	Finish of OBS deployment (Site#93-Site#110)
December 04	Airgun shooting (Line OGr1_obs)
December 05	Airgun shooting (Line OGr1_obs)
December 06	Airgun shooting (Line OGr1_obs)
December 07	Airgun shooting (Lines OGr1_obs and OGr1_obsR)
December 08	Airgun shooting (OGr1_obsR)
December 09	Airgun shooting (OGr1_obsR)
December 10	Airgun shooting (OGr1_obsR)
December 11	Finish of airgun shooting (Line OGr1_obsR) and OBS retrieval (Site#110-Site#93)
December 12	OBS retrieval (Site#94-Site#72)
December 13	OBS retrieval (Site#71-Site#64)
December 14	OBS retrieval (Site#63-Site#35)
December 15	Evacuation due to bad sea status
December 16	Evacuation due to bad sea status, transit and OBS retrieval (Site#34-Site#32)
December 17	OBS retrieval (Site#31-Site#4)
December 18	Finish of OBS retrieval (Site#4-Site#1) and G-gun shooting (Line KT4_s_1)
December 19	Transit and G-gun shooting (Line IBM2_ew_9)
December 20	G-gun shooting (Lines IBM2_ew_8 and IBM2_ew_5)
December 21	G-gun shooting (Line IBM2_ew_5)
December 22	Evacuation due to bad sea status and transit to the Tokyo Bay
December 23	Arrival at JAMSTEC

Table 2. Airgun shooting log.

OGr1_obs	Time (UTC)	Latitude (N)	Longitude (E)	SP
First shot	2007.12.4 2:51	24° 11.3077	142° 27.7899	991
First good shot	2007.12.4 2:55	24° 11.5241	142° 27.7769	995
Last good shot	2007.12.7 7:55	29° 35.8339	142° 9.7703	6991
Last shot	2007.12.7 7:55	29° 35.8339	142° 9.7703	6991

OGr1_obsR	Time (UTC)	Latitude (N)	Longitude (E)	SP
First shot	2007.12.7 9:38	29° 36.0663	142° 9.7426	6998
First good shot	2007.12.7 9:39	29° 35.9583	142° 9.7532	6996
Last good shot	2007.12.10 20:19	24° 11.2162	142° 27.7944	992
Last shot	2007.12.10 20:19	24° 11.2162	142° 27.7944	992

KT04_s_1	Time (UTC)	Latitude (N)	Longitude (E)	SP
First shot	2007.12.18 7:30	30° 38.9751	141° 29.8703	971
First good shot	2007.12.18 7:31	30° 39.0303	141° 29.8697	975
Last good shot	2007.12.18 20:26	31° 26.8984	141° 19.3088	4575
Last shot	2007.12.18 20:26	31° 26.8984	141° 19.3088	4575

IBM2_ew_9	Time (UTC)	Latitude (N)	Longitude (E)	SP
First shot	2007.12.19 4:34	31° 47.4708	141° 43.8508	976
First good shot	2007.12.19 4:34	31° 47.4726	141° 43.8189	978
Last good shot	2007.12.19 18:13	31° 44.2531	140° 39.6985	5033
Last shot	2007.12.19 18:13	31° 44.2531	140° 39.6985	5033

IBM2_ew_8	Time (UTC)	Latitude (N)	Longitude (E)	SP
First shot	2007.12.19 19:04	31° 45.8426	140° 39.5045	976
First good shot	2007.12.19 19:04	31° 45.8426	140° 39.5045	976
Leave from line	2007.12.20 4:38	31° 48.2198	141° 25.7628	3901
Shot stop	2007.12.20 5:16	31° 48.3580	141° 28.6900	4086
Shot restart	2007.12.20 8:19	31° 48.0287	141° 22.9663	3724
Shot restart on line	2007.12.20 8:27	31° 48.0836	141° 23.5815	2763
Last good shot	2007.12.20 12:59	31° 49.0675	141° 43.6748	5033
Last shot	2007.12.20 12:59	31° 49.0675	141° 43.6748	5033

IBM2_ew_5	Time (UTC)	Latitude (N)	Longitude (E)	SP
First shot	2007.12.20 15:41	31° 55.4192	141° 42.1048	976
First good shot	2007.12.20 15:41	31° 55.4192	141° 42.1048	976
Last good shot	2007.12.21 6:21	31° 52.2051	140° 37.8605	5033
Last shot	2007.12.21 6:21	31° 52.2051	140° 37.8605	5033

Ridge, Site62 in the southern part of the Ogasawara Ridge, and Site87 to the west of the zone of collision with the Ogasawara Plateau, as well as the horizontal components of Site60 are described in section 3.1. MCS data are described in section 3.2.

3.1 OBS

We retrieved 109 OBSs, and we were unable to retrieve one OBS due to problems with the transponder system. The data quality of the available OBSs was essentially good and we could trace the first phases on the vertical records up to a distance of 100-150 km from each OBS. The horizontal records also showed good quality despite having a poorer S/N ratio than the vertical ones. We saw converted S arrivals until a distance of about 100 km from the OBS. We describe the characteristics of the OBS data using the vertical record sections of Site5 (Figure 5), Site31 (Figure 6), Site62 (Figure 7), and Site87 (Figure 8) as follows.

Site5 was deployed on the northern Ogasawara Ridge. We can trace the refractions and reflections to the southern offset 150 km from the OBS (Figure 5). The apparent velocities of the first phases on the southern side are 3.0 km/s and 6.1 km/s at offsets of 3-6 km and 6-31 km, respectively. The first phases diminish and the reflections are identified at offsets of 25-41 km. At offsets of 40-60 km, first arrivals with an apparent velocity of 8.2 km/s are identified. Then, the phases break there, and other reflections are traced to an offset of 150 km. On the northern side, the apparent velocity reduces in comparison to that on the southern side due to the northward lean of the topography.

Site31 was deployed at the center of the Ogasawara Ridge. On the southern side, the first phases diminish at an offset of 42 km and clear reflections with a strong amplitude are marked from an offset of 30 km to 120 km (Figure 6). At the far southern side from 120 km, other reflections are identified at an offset of 170 km. The apparent velocities of the first phases are 3.7 km/s, 6.1 km/s, and 7.3 km/s at offsets of 2-6 km, 6-11 km, and 11-42 km, respectively. On the northern side, the first phases can be traced to an offset of 56 km and they diminish there. The apparent velocities of the first phases are 5.5 km/s, 6.6 km/s, 5.8 km/s, and 8.3 km/s at offsets of 4-14 km, 14-23 km, 23-40 km, and 40-50 km, respectively. On the far northern side, the latter phases can be traced to an offset of 120 km.

Site62 was deployed on the southern Ogasawara Ridge. The first phases on the southern and northern sides can be traced to offsets of 130 km and 90 km, respectively (Figure 7). The characteristics of this record section, namely, the apparent velocity of the first phases and distribution of the reflections, are obviously different from those of the OBSs deployed on the Ogasawara Ridge. On the southern side, the average apparent velocities of the first phases are 4.2 km/s, 4.7 km/s, 5.3 km/s, 6.1 km/s, 4.9 km/s, 6.1 km/s, 6.9 km/s, and 8.2 km/s at offsets of 2-8 km, 8-15 km, 15-21 km, 21-37 km, 51-61 km, 61-71 km, 71-86 km, and 114-137 km, respectively. On the northern side, the apparent velocities of the first phases are 3.1 km/s, 5.5 km/s, and 4.8 km/s at offsets of 1-4 km, 4-13 km, and 13-32 km respectively. The first phases on the far northern side have a meandering apparent velocity, and the average velocity is about 8.4 km/s.

Site87 was deployed in the forearc region of the southern end of the Izu-Ogasawara arc. The first phases on both sides are traced to an offset of 120 km (Figure 8). On the southern side, the apparent velocities of first phases are 3.5 km/s, 4.5 km/s, 6.7 km/s, 6.9 km/s, 7.5 km/s, and 9.4 km/s at offsets of 4-7 km, 7-11 km, 11-21 km, 21-71 km, 71-102 km, and 102-115 km, respectively. On the northern side, the apparent velocities of the first phases are 4.1 km/s, 7.1 km/s, 6.2 km/s, and 8.7 km/s at offsets of 4-9 km, 9-30 km, 30-50 km, and 50-80 km, respectively. Clear reflections can be seen at offsets of 15-30 km and 60-100 km.

3.2 MCS

The MCS data recorded by the multichannel hydrophone streamer have sufficient quality to enable an understanding of shallow structures. The MCS profile using an airgun array with a shot interval of 200 m (line OGr1_obs) is shown in Figure 9. The MCS profiles using a G-gun array with a shot interval of 25 m (lines KT04_s_1, IBM2_ew_9, IBM2_ew_8, and IBM2_ew_5) are shown in Figures 10, 11, 12, and 13, respectively. The applied tentative flows were editing of bad quality traces, static shift, resampling for MCS surveys with the G-gun array, geometry set, prefiltering with bandpass (3-5-103-125 Hz for airgun shooting and 9-14-240-250 Hz for G-gun shooting), collection of spherical divergence, predictive deconvolution filtering (predictive distance of 25 ms for airgun shooting and 16 ms for G-gun shooting; operator length of 240 ms

Table 3. OBS information.

Site	Deployment				Estimated position by SSBL			Retrieval			
	Time	Coordinate						Time	Coordinate		
	UTC	Latitude (N)	Longitude (E)	Dep.(m)	Latitude (N)	Longitude (E)	Dep.(m)	UTC	Latitude (N)	Longitude (E)	Dep.(m)
1	11/27 13:20	29°21.7707'	142°10.6008'	4795	29°21.6487'	142°10.5876'	4707	12/17 20:59	29°21.3754'	142°10.8566'	4800
2	11/27 14:51	29°19.0766'	142°10.7675'	4780	29°19.0164'	142°10.8089'	4679	12/17 19:36	29°18.6849'	142°11.0521'	4791
3	11/27 16:22	29°16.3634'	142°10.9035'	4725	29°16.3327'	142°10.9322'	4636	12/17 18:54	29°16.0912'	142°11.2167'	4701
4	11/27 17:51	29°13.6623'	142°11.0629'	4473	29°13.5688'	142°11.0791'	4392	12/17 17:54	29°13.3387'	142°11.2694'	4402
5	11/27 19:17	29°10.9690'	142°11.2221'	4060	29°10.9221'	142°11.2145'	3974	12/17 17:04	29°10.6437'	142°11.3240'	4006
6	11/27 20:40	29°08.2729'	142°11.3782'	3889	29°08.1166'	142°11.2543'	3843	12/17 16:10	29°07.9376'	142°11.3852'	3857
7	11/27 22:08	29°05.5863'	142°11.5367'	3831	29°05.4635'	142°11.3998'	3775	12/17 15:27	29°05.2606'	142°11.4778'	3820
8	11/27 23:33	29°02.8836'	142°11.7537'	3899	29°02.7925'	142°11.6571'	3861	12/17 14:40	29°02.6033'	142°11.6880'	3884
9	11/28 0:56	29°00.1936'	142°11.8983'	3773	29°00.1223'	142°11.8382'	3729	12/17 13:58	28°59.9490'	142°11.8363'	3751
10	11/28 2:18	28°57.5025'	142°12.0574'	3648	28°57.4349'	142°12.0110'	3613	12/17 13:15	28°57.2730'	142°12.0417'	3637
11	11/28 3:42	28°54.8012'	142°12.2159'	3525	28°54.7702'	142°12.1467'	3488	12/17 12:31	28°54.6241'	142°12.1047'	3488
12	11/28 5:05	28°52.1052'	142°12.3433'	3265	28°52.0684'	142°12.2576'	3278	12/17 11:49	28°51.9769'	142°12.2507'	3235
13	11/28 6:27	28°49.4219'	142°12.5878'	2930	28°49.3595'	142°12.4311'	2913	12/17 11:03	28°49.3025'	142°12.4368'	2905
14	11/28 7:43	28°46.7235'	142°12.7500'	2739	28°46.6749'	142°12.5511'	2737	12/17 10:14	28°46.6174'	142°12.5341'	2745
15	11/28 8:57	28°44.0405'	142°12.9030'	2683	28°44.0245'	142°12.6843'	2656	12/17 9:29	28°43.9271'	142°12.6621'	2651
16	11/28 10:10	28°41.2869'	142°13.0889'	2500	28°41.3146'	142°12.8726'	2491	12/17 8:47	28°41.2434'	142°12.8559'	2502
17	11/28 11:19	28°38.5992'	142°13.2340'	2399	28°38.6489'	142°13.0577'	2392	12/17 7:59	28°38.5749'	142°13.0388'	2384
18	11/28 12:28	28°35.8918'	142°13.3776'	2164	28°35.9652'	142°13.2652'	2167	12/17 7:17	28°35.8975'	142°13.2463'	2169
19	11/28 13:34	28°33.2229'	142°13.5082'	2100	28°33.3139'	142°13.4040'	2105	12/17 6:35	28°33.1992'	142°13.4455'	2105
20	11/28 14:41	28°30.4815'	142°13.6367'	1943	28°30.5463'	142°13.5968'	1945	12/17 5:58	28°30.4847'	142°13.5981'	1939
21	11/28 15:47	28°27.7938'	142°13.7637'	1883	28°27.8688'	142°13.7415'	1875	12/17 5:18	28°27.7873'	142°13.7917'	1873
22	11/28 16:50	28°25.1235'	142°13.9309'	1883	28°25.1797'	142°13.9339'	1887	12/17 4:42	28°25.1349'	142°13.9706'	1880
23	11/28 17:51	28°22.4544'	142°14.0787'	1881	28°22.4933'	142°14.0763'	1881	12/17 4:04	28°22.4491'	142°14.1028'	1877
24	11/28 18:50	28°19.7667'	142°14.2353'	1883	28°19.7833'	142°14.2114'	1888	12/17 3:30	28°17.7278'	142°14.2873'	1884
25	11/28 19:45	28°17.0742'	142°14.4083'	1839	28°17.0490'	142°14.4238'	1840	12/17 2:53	28°17.0258'	142°14.4388'	1832
26	11/28 20:42	28°14.3875'	142°14.5530'	1809	28°14.4022'	142°14.4629'	1803	12/17 2:06	28°14.3498'	142°14.4749'	1793
27	11/28 21:42	28°11.6207'	142°14.7508'	1660	28°11.6391'	142°14.6465'	1713	12/17 1:16	28°11.5931'	142°14.6677'	1666
28	11/28 22:39	28°08.9755'	142°14.9041'	1566	28°08.9680'	142°14.8351'	1578	12/17 0:31	28°08.9158'	142°14.8504'	1568
29	11/28 23:37	28°06.2516'	142°15.0400'	1455	28°06.3032'	142°14.9543'	1479	12/16 23:48	28°06.2338'	142°14.9532'	1470
30	11/29 10:18	28°03.5772'	142°15.0692'	1420	28°03.6212'	142°15.0144'	1413	12/16 23:00	28°03.5659'	142°14.9523'	1415
31	11/29 11:10	28°00.9083'	142°15.2260'	1309	28°00.9844'	142°15.2199'	1290	12/16 22:03	28°00.8854'	142°15.1938'	1303
32	11/29 12:01	27°58.2440'	142°15.3671'	1186	27°58.3485'	142°15.3795'	1185	12/16 20:59	27°58.2936'	142°15.4335'	1178
33	11/29 12:50	27°55.5655'	142°15.5130'	1096	27°55.6972'	142°15.5044'	1068	12/16 19:34	27°55.6304'	142°15.5817'	1090
34	11/29 13:40	27°52.7767'	142°15.6895'	940	27°52.8356'	142°15.7145'	924	12/16 17:34	27°52.1299'	142°15.8207'	976
35	11/29 14:26	27°50.0888'	142°15.8304'	882	27°50.1519'	142°15.8392'	873	12/13 17:56	27°50.1246'	142°15.9304'	883
36	11/29 15:09	27°47.3751'	142°16.0042'	760	27°47.4012'	142°16.0398'	754	12/13 17:00	27°47.3717'	142°16.1152'	744
37	11/29 15:53	27°44.7090'	142°16.1265'	684	27°44.7084'	142°16.1724'	704	12/13 16:09	27°44.7057'	142°16.2283'	682
38	11/29 16:35	27°42.0420'	142°16.2706'	595	27°42.0273'	142°16.3027'	596	12/13 15:25	27°42.0288'	142°16.4145'	581
39	11/29 17:14	27°39.3893'	142°16.4215'	325	27°39.3598'	142°16.4512'	317	12/13 14:35	27°39.4247'	142°16.5530'	343
40	11/29 17:48	27°36.6486'	142°16.5755'	242	27°36.6255'	142°16.5925'	247	12/13 13:49	27°36.7163'	142°16.8572'	261
41	11/29 18:19	27°33.9777'	142°16.7480'	270	27°33.9535'	142°16.7581'	269	12/13 13:06	27°34.1109'	142°16.9871'	280
42	11/29 18:47	27°31.3080'	142°16.9097'	350	27°31.2651'	142°16.9568'	305	12/13 12:25	27°31.3815'	142°17.1560'	340
43	11/29 19:18	27°28.6060'	142°17.0506'	374	27°28.5705'	142°17.0603'	392	12/13 11:41	27°28.6359'	142°17.1400'	394
44	11/29 19:50	27°25.9390'	142°17.2140'	656	27°25.9146'	142°17.2062'	650	12/13 10:58	27°25.9408'	142°17.2454'	658
45	11/29 20:23	27°23.2313'	142°17.3764'	349	27°23.2164'	142°17.3671'	344	12/13 10:14	27°23.2634'	142°17.3539'	346
46	11/29 20:54	27°20.5259'	142°17.5040'	322	27°20.5137'	142°17.4866'	324	12/13 9:25	27°20.5425'	142°17.4545'	317
47	11/29 21:26	27°17.8201'	142°17.6483'	276	27°17.8054'	142°17.6382'	277	12/13 8:43	27°17.8506'	142°17.6535'	273
48	11/29 22:00	27°15.0790'	142°17.7930'	498	27°15.0800'	142°17.8026'	495	12/13 8:03	27°15.0915'	142°17.8044'	496
49	11/29 22:36	27°12.4029'	142°17.9619'	656	27°12.4071'	142°17.9621'	660	12/13 7:24	27°12.4515'	142°17.9820'	665
50	11/29 23:12	27°09.6789'	142°18.1162'	551	27°09.6710'	142°18.0983'	547	unrecovered	-	-	-
51	11/29 23:50	27°06.9980'	142°18.2621'	231	27°06.9961'	142°18.2473'	219	12/13 5:39	27°07.0116'	142°18.1990'	225
52	11/30 0:27	27°04.3175'	142°18.4147'	211	27°04.3241'	142°18.4013'	230	12/13 4:55	27°04.3513'	142°18.3313'	208
53	11/30 1:05	27°01.6194'	142°18.5760'	801	27°01.5984'	142°18.5230'	814	12/13 3:55	27°01.5988'	142°18.3963'	809
54	11/30 1:50	26°58.8989'	142°18.7130'	1161	26°58.9203'	142°18.6868'	1171	12/13 3:03	26°58.9787'	142°18.7908'	1156
55	11/30 2:40	26°56.2433'	142°18.8806'	1448	26°56.2545'	142°18.8798'	1434	12/13 2:15	26°56.2802'	142°19.0259'	1415
56	11/30 6:18	26°53.6195'	142°19.0362'	1348	26°53.5878'	142°19.0233'	1340	12/13 1:36	26°53.5928'	142°19.1657'	1346
57	12/1 7:19	26°50.8701'	142°19.1690'	1251	26°50.8436'	142°19.1715'	1248	12/13 0:56	26°50.8695'	142°19.2125'	1258
58	12/1 8:16	26°48.1883'	142°19.3005'	871	26°48.1687'	142°19.2937'	873	12/13 0:16	26°48.1909'	142°19.3311'	868
59	12/1 9:10	26°45.4436'	142°19.4758'	644	26°45.4271'	142°19.5062'	631	12/12 23:36	26°45.4862'	142°19.5199'	662
60	12/1 10:04	26°42.7643'	142°19.5995'	386	26°42.7505'	142°19.5868'	386	12/12 23:00	26°42.7767'	142°19.5815'	620
61	12/1 10:51	26°40.0707'	142°19.7429'	527	26°40.0568'	142°19.7508'	534	12/12 22:25	26°40.0875'	142°19.7314'	517
62	12/1 11:39	26°37.3793'	142°19.9004'	642	26°37.3675'	142°19.9026'	635	12/12 21:44	26°37.3750'	142°19.8811'	637
63	12/1 12:28	26°34.6985'	142°20.0609'	467	26°34.6854'	142°20.0643'	464	12/12 21:03	26°34.7100'	142°20.0472'	465
64	12/1 13:17	26°32.0144'	142°20.1885'	605	26°32.0404'	142°20.1717'	583	12/12 19:22	26°32.0924'	142°20.1599'	615
65	12/1 14:06	26°29.3021'	142°20.3196'	961	26°29.2897'	142°20.3082'	915	12/12 19:38	26°29.2943'	142°20.3196'	960
66	12/1 14:59	26°26.6130'	142°20.4875'	1059	26°26.5797'	142°20.5267'	1065	12/12 18:56	26°26.6028'	142°20.4930'	1056
67	12/1 15:57	26°23.9058'	142°20.6023'	1100	26°23.8786'	142°20.6348'	1108	12/12 18:13	26°23.8949'	142°20.6158'	1094
68	12/1 16:51	26°21.1983'	142°20.7334'	1229	26°21.1984'	142°20.7699'	1228	12/12 17:30	26°21.2452'	142°20.7363'	1222
69	12/1 17:47	26°18.5107'	142°20.9014'	1263	26°18.4758'	142°20.9099'	1285	12/12 16:45	26°18.5870'	142°20.9092'	1253
70	12/1 18:44	26°15.8208'	142°21.0686'	1013	26°15.7765'	142°21.0728'	1001	12/12 16:03	26°15.8540'	142°21.1020'	1008
71	12/1 19:34	26°13.1329'	142°21.2223'	1350	26°13.0953'	142°21.2175'	1394	12/12 15:22	26°13.2308'	142°21.3626'	1317
72	12/1 20:29	26°10.4274'	142°21.3762'	1564	26°10.4069'	142°21.3371'	1581	12/12 14:33	26°10.5526'	142°21.4089'	1549
73	12/1 21:27	26°07.7289'	142°21.5129'	1779	26°07.7059'	142°21.4367'	1785	12/12 13:48	26°07.8292'	142°21.4820'	1771
74	12/1 22:24	26°05.0817'	142°21.6962'	2190	26°05.0500'	142°21.6171'	2197	12/12 13:00	26°05.1516'	142°21.5942'	2180
75	12/1 23:26	26°02.3895'	142°21.8294'	2491	26°02.2994'	142°21.5936'	2523	12/12 12:05	26°02.3814'	142°21.4560'	2535
76	12/2 0:35	25°59.7078'	142°22.0628'	2717	25°59.6823'	142°21.9157'	2651	12/12 10:59	25°59.7141'	142°21.7220'	2743
77	12/2 1:50	25°56.9772'	142°22.2963'	2685	25°56.9650'	142°22.1495'	2680	12/12 10:06	25°56.9709'	142°22.0036'	2669
78	12/2 3:04	25°54.3158'	142°22.3876'	2658	25°54.3118'	142°22.3305'	2598	12/12 9:26	25°54.3042'	142°22.0861'	2601
79	12/2 4:17	25°51.5955'	142°22.4468'	2579	25°51.5600'	142°22.3665'	2572	12/12 8:36	25°51.5775'	142°22.1634'	2576
80	12/2 5:33	25°48.8836'	142°22.6211'	2179	25°48.8574'	142°22.5582'	2178	12/12 7:55	25°48.8720'	142°22.3750'	2212
81	12/2 6:44	25°46.2044'	142°22.7448'	2148	25°46.1915'	142°22.6769'	2134	12/12 7:09	25°46.1982'	142°22.5058'	2116
82	12/2 7:58	25°43.4741'	142°22.9315'	2207	25°43.4949'	142°22.8762'	2196	12/12 6:22	25°43.4890'	142°22.7362'	2199
83	12/2 9:17	25°40.8224'	142°22.9989'	2396	25°40.8382'	142°22.9220'	2400	12/12 5:42	25°40.8555'	142°22.8028'	2405
84	12/2 10:34	25°38.1069'	142°23.1574'	2475	25°38.1082'	142°23.0793'	2489	12/12 4:55	25°38.1117'	142°22.9709'	2485
85	12/2 11:47	25°35.3983'	142°23.3188'	2508	25°35.4297'	142°23.1966'	2504	12/12 4:06	25°35.4185'	142°23.1548'	2511
86	12/2 13:01	25°32.7042'	142°23.4313'	2504	25°32.7251'	142°23.3228'	2488	12/12 3:18	25°32.7235'	142°23.2890'	2500
87	12/2 14:15	25°29.6867'	142°23.6397'	2467	25°30.0366'	142°23.5334'	2470	12/12 2:29	25°30.0503'	142°23.4779'	2472
88	12/2 15:30	25°27.2864'	142°23.7811'	2449	25°27.3473'	142°23.6724'	2451	12/12 1:40	25°27.3661'	142°23.6541'	2454
89	12/2 16:49	25°24.5677'	142°23.9282'	2414	25°24.6272'	142°23.8877'	2416	12/12 0:48	25°24.6640'	142°23.8094'	2418
90	12/2 18:01	25°21.8817'	142°24.0565'	2303	25°21.9605'	142°23.9916'	2301	12/11 23:50	25°22.0305'	142°23.9493'	2311
91	12/2 19:03	25°19.1677'	142°24.1992'	2249	25°19.2233'	142°24.1550'	2258	12/11 22:46	25°19.3425'	142°24.0832'	2254
92	12/2 20:02	25°16.4799'	142°24.3614'	2081	25°16.5349'	142°24.3273'	2081	12/11 21:31	25°16.6861'	142°24.2300'	2087
93	12/2 20:58	25°13.7966'	142°24.5089'	2142	25°13.8455'	142°24.4726'	2133	12/11 20:37	25°14.0031'	142°24.3568'	2051
94	12/2 21:55	25°11.0432'	142°24.6767'	2160	25°11.0903'	142°24.6307'	2176	12/11 19:46	25°11.3097'	142°24.5053'	2139
95	12/2 22:50	25°08.4002'	142°24.7824'	2204	25°08.4434'	142°24.7312'	2201	12/11 18:53	25°08.6294'	142°24.5800'	2197
96	12/2 23:49	25°05.6831'	142°24.9335'	2089	25°05.7306'	142°24.8930'	2072	12/11 17:57	25°05.8686'	142°24.7652'	1959
97	12/3 0:48	25°03.0100'	142°25.0849'	2117	25°03.0629'	142°25.0270'	2074	12/11 17:04	25°03.2027'	142°24.8920'	2044
98	12/3 1:48	25°00.3138'	142°25.2142'	2121	25°00.3717'	142°25.1718'	2118	12/11 16:15	25°00.5270'	142°25.0087'	2024
99	12/3 2:48	24°57.6138'	142°25.3736'	2112	24°57.6571'	142°25.3174'	2103	12/11 15:20	24°57.7975'	142°25.1745'	2076
100	12/3 3:50	24°54.9332'	142°25.5301'	2246	24°54.9911'	142°25.5046'	2247	12/11 14:26	24°55.1511'	142°25.3350'	2225
101	12/3 5:00	24°52.2587'	142°25.6672'	2591	24°52.3028'	142°25.6401'	2594	12/11 13:31	24°52.4656'	142°25.5293'	2602
102	12/3 6:12	24°49.5749'	142°25.7464'	2576	24°49.6305'	142°25.7221'	2577	12/11 12:22	24°49.7583'	142°25.5989'	2577
103	12/3 7:22	24°46.8911'	142°25.8904'	2688	24°46.9863'	142°25.8714'	2672	12/11 11:15	24°47.0924'	142°25.7496'	2677
104	12/3 8:30	24°44.1263'	142°26.0770'	2792	24°44.1723'	142°26.0768'	2790	12/11 10:04	24°44.2549'	142°25.9806'	2788
105	12/3 9:36	24°41.4997'	142°26.2100'	2842	24°41.5344'	142°26.2199'	2841	12/11 8:53	24°41.6175'	142°26.1004'	2837
106	12/3 10:42	24°38.8029'	142°26.3589'	2865	24°38.8361'	142°26.3618'	2867	12/11 7:46	24°38.8647'	142°26.2788'	2865
107	12/3 11:56	24°36.0977'	142°26.4918'	2876	24°36.0835'	142°26.4562'	2877	12/11 6:28	24°36.1301'	142°26.3983'	2876
108	12/3 13:08	24°33.4091'	142°26.6597'	2881	24°33.4229'	142°26.6543'	2881	12/11 5:18	24°33.4403'	142°26.5859'	2877
109	12/3 14:19	24°30.7100'	142°26.7831'	2828	24°30.7291'	142°26.8127'	2824	12/11 3:59	24°30.7202'	142°26.7991'	2842
110	12/2 15:29	24°28.0292'	142°26.9342'	2655	24°28.0524'	142°26.9356'	2658	12/11 2:41	24°28.0387'	142°26.9534'	2679

for airgun shooting and 120 ms for G-gun shooting), brute stacking with constant velocity of 1,500 m/s, and stolt migration using the constant velocity. For the reflection data along line OGr1_obs, we set bins with sizes of 62.5 m due to the sparse shot interval.

On the northernmost side (CMP: 0-3,000), there exist three gentle topographic highs at CMPs of 450, 1,500, and 2,850, and these correspond to en-echelon structures with a NNE-SSW strike (Figure 1). Between these highs, sedimentary layers with a maximum thickness of approximately 0.5 s are distributed, and they do not seem to be deformed by tectonic stresses. On the other hand, it is suggested that the topographic high (CMP: 3,400-6,400) with extreme unevenness originates from relatively large–scale tectonic stresses with a direction along the N-S component, because the shape of the basement is similar to that of the topography. Although the phases parallel to the sea bottom located 0.2 s below the seafloor can probably be identified as babbles of the airgun source signals, the phases located 0.4-0.6 s below the seafloor can be traced as an interface in the shallow structure roughly parallel to the seafloor. On the southern half (CMP: 6,400-9,500), the slope gently decline southward and the sedimentary layers with acoustic transparency are very thin, except at CMP 7,300-7,400. Some northward leaning events seem to develop below the basement at CMP 8,200-8,800, and advanced processing should be carried out to clearly identify them.

Line KT04_s_1 runs on the forearc basin in the direction of NNW-SSE. It appears that homogenous sediments are distributed beneath this line (Figure 10). Although the thickness of the sediments varies from about 0.5 to 1.0 s, except in the case of CMP 4,600-5,600, the events within the sedimentary layers do not seem to be deformed. This suggests that the tectonic stress along the N-S direction may be small.

Line IBM2_ew_9 runs in the forearc region in the E-W direction. Although sediments with a thickness of about 0.5-1.5 s cover the whole seismic line (Figure 11), they become thinner on the eastern side from CDP 4,000. The events within the sedimentary layer are not likely deformed. On the other hand, we identify a deepening of the basement and thick sediments, suggesting past crustal rifting at CDP 6,400.

Line IBM2_ew_8 also runs in the forearc region parallel to line IBM2_ew_9. The characteristics of the reflection records are almost the same as those of line IBM2_ew_9 (Figure 12). Thick and thin sediments develop on the western and eastern sides, respectively. The maximum thickness of the sediments at CDP 0-1,000 is approximately 2 s. Deepening of the basement is also common to line IBM2_ew_9 at CDP 1,800.

Line IBM2_ew_5 also runs E-W like line IBM2_ew_9. Although the characteristics of the reflection records are common to line IBM2_ew_9, the sediments at CDP 7,200-6,000 are thicker than those along line IBM2_ew_9 (Figure 13). The maximum thickness of the sediments at CDP 7,000-6,800 is approximately 2.5 s. Deepening of the basement is identified as being similar to that in the case of line IBM2_ew_9 at CDP 6,900.

4. Summary

We carried out the large active seismic experiments using 110 OBSs, a large airgun array with a total capacity of 12,000 cu. in., and a 12-channel hydrophone streamer. The qualities of OBS and MCS data were good enough to understand the velocity structure and to discuss the crustal growth in this area. The OBSs recorded clear phases at offsets of 150-200 km from each OBS. A part of the horizontal components of OBSs was also good and the converted S-waves could be recorded at offsets of over 100 km. The MCS data indicate the variation of the sedimentary structures, the topography of the basement, and the configuration of the faults that developed within the rift zone. We will construct a velocity model and investigate structural variation that suggests crustal heterogeneity due to difference in age. In addition, we will study the relationship between the crustal growth and the crustal rifting.

Acknowledgements

We greatly appreciate to following members of the KY0715 cruise shipboard party and we would not have been able to successfully conduct this seismic experiment without their efforts. We thank Seiichi Miura, Mikiya Yamashita, Takeshi Sato and Yuka Kaiho for planning discussion of this cruise and support during the cruise.

Marine technicians

Chief Technician Makoto Ito

Technician	Ikumasa Terada
Technician	Nobuo Kojima
Technician	Ayumi Mizota
Technician	Miho Ido
Technician	Kimiko Serizawa
Technician	Yuta Watarai
Technician	Ami Iwaki
Technician	Mitsuteru Kuno
Technician	Takuya Maekawa
Technician	Hiroyoshi Shimizu
Technician	Masaki Konno
Technician	Tetsuya Inaba

Crew

Captain	Fusao Saitoh
Chief Officer	Rikita Yoshida
Second Officer	Kenta Oya
Junior Second Officer	Kazunori Kamiya
Third Officer	Tetsuo Shirayama
Chief Engineer	Toshihiro Kimura
First Engineer	Masaya Sumida
Second Engineer	Shigenobu Maruyama
Third Engineer	Saburo Sakaemura
Chief Radio Officer	Masamoto Takahashi
Second Radio Officer	Yusuke Takeuchi
Third Radio Officer	Hiroki Ishiwata
Boatswein	Kazuo Abe
Able seaman	Kazumi Ogasawara
Able seaman	Osamu Tokunaga
Able seaman	Kinya Shoji
Able seaman	Shuichi Yamamoto
Able seaman	Nobuyuki Ichikawa
Sailor	Myuta Yamazaki
No.1 Oiler	Masayuki Masunaga
Oiler	Takeshi Fukubara
Oiler	Tomoyuki Hashimoto
Assistant Oiler	Masanori Ueda
Assistant Oiler	Sota Misago
Chief Steward	Kaoru Takashima
Steward	Shigeto Ariyama
Steward	Kazuhiro Hirayama
Steward	Junichi Shiki
Steward	Akihide Saito
Jr. Third Officer	Kazuki Miyake
Sailor	Takuya Miyashita

Reference

Crawford, A. J., L. Beccaluva and G. Serri. (1981), Tectomagmatic evolution of the West Philippine - Mariana region and the origin of boninites, *Earth Planets. Sci. Lett., 54*, 346-356.

Fujioka, K., W. Tokunaga, H. Yokose, J. Kasahara, T. Sato, R. Miura and T. Ishii(2005), Hahajima Seamount: An enigmatic tectonic block at the junction between the Izu-Bonin and Mariana Trenches, *The Island Arc, 14*, 616-622.

Hall, R., J. R., Ali, C. D. Anderson, and S. J. Baker(1995), Origin and motion history of the Philippine Sea Plate, *Tectonophysics, 251*, 229-250.

Honza, E. and K. Fujioka (2004), Formation of arcs and backarc basins inferred from the tectonic evolution of southeast Asia since the late Cretaceous, *Tectonophysics, 384*, 23-53.

Ishizuka, O., J. Kimura, Y. B. Li, R. J. Stern, M. K. Reagan, R. N. Taylor, Y. Ohara, S. H. Bloomer, T. Ishii, U. S. Hargrove III and S. Haraguchi(2006), Early stages in the evolution of Izu-Bonin arc volcanism: New age, chemical, and isotopic constraints, *Earth Planets. Sci. Lett., 250*, 385-401.

Kaiho, Y., N. Takahashi, T. Sato, G. Fujie, S. Kodaira and Y. Kaneda(2005), Wide-angle seismic profiling of oceanic island arc in the southern Izu-Ogasawara arc -KY0502 cruise-, *JAMSTEC rep. Res. Dev., 3*, 43-52.

Kanazawa,T and H. Shiobara (1994), Newly developed ocean bottom seismometer, *Prog. Abst. Japan Earth and Planetary Science Meeting, 2*, 240.

Karig, D. E. and G. F. Moore(1975), Tectonic complexities in the Bonin arc system, *Tectonophysics, 27*, 97-118.

Kodaira, S., T. Sato, N. Takahashi, A. Ito, Y. Tamura, Y. Tatsumi and Y. Kaneda(2007), Seismological evidences for variation of continental growth along the Izu intra-oceanic arc and its implication for arc volcanism, *J. Geophys. Res., 112*, B05104, doi:10.1029/2006JB004593.

Macpherson, C. G. and R. Hall(2001), Tectonic setting of Eocene boninite magmatism in the Izu-Bonin-Mariana forearc, *Earth Planet. Sci. Lett., 186*, 215-230.

Shinohara, M., K. Suyehiro, S. Matsuda and K. Ozawa(1993), Digital recording ocean bottom seismometer using portable digital audio tape recorder. *J. Jpn. Soc. Mar. Surv. Tech., 5*, 21-31. (Japanese with English abstract)

Stern, R. J. and S. H. Bloomer(1992), Subduction zone infancy: Examples from the Eocene Izu-Bonin-Mariana and Jurassic California arcs, *Geol. Soc. Am. Bull.*, *104*, 1621-1636.

Suyehiro, K., N. Takahashi, Y. Ariie, Y. Yokoi, R. Hino, M. Shinohara, T. Kanazawa, N. Hirata, H. Tokuyama, and A. Taira(1996), Continental crust, crustal underplating, and low-Q upper mantle beneath an oceanic island arc, *Science*, *272*, 390-392.

Takahashi, N., K. Suyehiro and M. Shinohara (1998), Implications from the seismic crustal structure of the northern Izu-Ogasawara arc, *Island arc*, *7*, 383-394.

Takahashi, N. S. Kodaira, A. Ito, H. Shiobara, H. Sugioka, B. Kerr, I. Vlad, S. Klemperer, Y. Kaneda and K. Suyehiro (2003), Deep seismic profiling across the Mariana arc - backarc system, *JAMSTEC J. Deep Sea Res.*, *23*, 55-68.

Takahashi, N., S. Kodaira, Y. Tatsumi, M. Yamashita, T. Sato, Y. Kaiho, S. Miura, T. No, K. Takizawa and Y. Kaneda, Structural variations of arc crusts and rifted margins in the southern Izu-Ogasawara arc-back arc system, G-cubed (submitted).

Tatsumi, Y. (2000), Slab melting: its role in continental crust formation and mantle evolution, *Geophys. Res. Lett.*, *27*, 23, 3941-3944,.